Journal of Materials Chemistry C

ROYAL SOCIETY OF CHEMISTRY

PAPER

View Article Online
View Journal | View Issue

Cite this: J. Mater. Chem. C, 2023, 11, 5770

Copper assisted symmetry and size control of gold nanobars†

Weilun Li,[a] Wenming Tong, ‡[bc] Joanne Etheridge *[ade] and Alison M. Funston *[bc]

Received 12th December 2022,
Accepted 28th March 2023

DOI: 10.1039/d2tc05286e

rsc.li/materials-c

Shape and size control of metal nanocrystals has become a powerful tool in tuning their physicochemical properties for applications, however, the growth mechanisms controlling shape and size are not fully elucidated. Gold nanocuboids provide a simple nanoparticle system for investigating nanocrystal growth mechanisms. Here, we study the control over size and shape anisotropy of gold nanocuboids by copper additives. We first optimize the synthesis and yield. We find that, in the presence of copper additives, symmetry is broken and anisotropic growth can occur, leading to nanobars, rather than nanocubes, accompanied by a significant reduction in particle size. We show that symmetry breaking is caused by a combination of rapid deposition on {111} facets coupled with the slow surface diffusion rate introduced by surface copper. This reveals a mechanism by which metal additives can cause symmetry breaking and control shape in nanoparticle growth.

Introduction

Noble metal nanocrystals have attracted wide attention owing to their highly tunable properties, which are dependent on their shape, size, and composition. In particular, the symmetry of nanocrystal shape is one of the intrinsic factors that directly influence the optical, chemical, and electrical properties of the nanocrystals by changing the electronic structures.[1] Understanding the mechanism(s) that enable particle symmetry to be changed during nanocrystal growth is critical for understanding how to control the shape, and therefore the optical response, of the final product. However, studies of the symmetry breaking and growth mechanisms have been hindered by the multitude of parameters involved in nanocrystal syntheses.

Gold nanocubes represent perhaps the simplest example of cubic systems. They are generally observed to be single crystals bounded by six equivalent {001} facets, reflecting the symmetry of the gold unit cell.[2–4] This simple structure has made gold nanocubes attractive as a fundamental system to study nanocrystal growth, such as facet formation,[5,6] core–shell structures[7–9] and symmetry breaking.[10] It is also a central geometry in the applications of self-assembly,[11] cell imaging,[12,13] plasmon coupling[14,15] and surface-enhanced Raman spectroscopy.[16,17] Gold nanocubes in high yield were first synthesized *via* the seed-mediated method with excellent control over nanocube sizes.[18] Other seedless methods[5] and electrochemical methods[19] have also successfully produced gold nanocubes. The key to the synthesis of gold nanocubes is to preserve {100} facets. A critical component is the {100}-type capping agents, which are thought to specifically bind to the {100} facets and reduce their surface energies.[20] The small gold nanocrystals used as seeds are single crystal cuboctahedra.[21] If these seeds are to grow in the growth solution, cubes will result if the growth rates along the ⟨100⟩ directions are much slower than the ⟨111⟩ directions, so faster growth along the ⟨111⟩ directions will lead to the disappearance of {111} facets.

For the seed-mediated growth of gold nanocubes with cetyltrimethylammonium bromide (CTAB) as a growth-directing surfactant, there is a critical size range (25–27 nm) at which the transformation of quasi-spherical to cubic shape occurs.[6] The synthesis produces stable cubes in high yield with sizes larger than ~45 nm.[6] These cubes are highly regular, with little deviation from cubic (O_h) symmetry with the exception of some truncation at the vertices and edges.[6,18] Cubes of smaller size have been observed in similar syntheses when foreign metal ions are introduced into the growth solution. For example, in the presence of Cu^{2+} the formation of small gold nanocubes (~35 nm) with reasonably high yield is achieved.[22] Interestingly,

[a] Department of Materials Science and Engineering, Monash University, Clayton, Victoria, 3800, Australia. E-mail: joanne.etheridge@monash.edu
[b] School of Chemistry, Monash University, Clayton, Victoria, 3800, Australia. E-mail: alison.funston@monash.edu
[c] ARC Centre of Excellence in Exciton Science, Monash University, Clayton, Victoria, 3800, Australia
[d] Monash Centre for Electron Microscopy, Monash University, Clayton, Victoria, 3800, Australia
[e] School of Physics and Astronomy, Monash University, Clayton, Victoria, 3800, Australia

† Electronic supplementary information (ESI) available. See DOI: https://doi.org/10.1039/d2tc05286e

‡ Present address: School of Biological and Chemical Sciences and Energy Research Centre, Ryan Institute, University of Galway, H91 TK33, Galway, Ireland.

these nanocubes (Cu^{2+}-assisted) were measured to have aspect ratios (AR = length/width) larger than 1, indicating the breaking of cubic symmetry (O_h to D_{2h}). Strictly, these should be called nanobars, and we will use this terminology hereon to describe a cuboid with AR $\neq$ 1. Small cubes/bars (20–30 nm) are also formed as minor byproducts in gold nanorod synthesis in the presence of Ag^+, benzyldimethylhexadecylammonium chloride (BDAC), and CTAB.[23]

It is remarkable that gold can grow into nanobars. This implies that the growth rate along nominally symmetry-equivalent directions is different! In this paper, we seek to understand why this is so and the role of copper in this process.

The function of foreign metal ions in gold nanoparticle growth has been described in terms of underpotential deposition (UPD). Gold nanorod syntheses with silver ions are probably the most widely studied systems with metal additives. Here the silver ions are proposed to deposit preferentially on high index facets of gold nanoparticles *via* UPD. These high index facets become less accessible for further deposition, known as the surface passivation mechanism.[24–26] In contrast, the role of copper ions as additives has rarely been investigated. In particular, it remains unclear as to how the anisotropic growth of gold nanobars is induced by the presence of copper ions, and how the cuboid shapes are stabilized and formed at relatively smaller sizes. Mechanisms proposed in the literature to account for the roles of Cu^{2+} additives, including selective surface passivation,[22,27] oxidative etching[28,29] and galvanic replacement,[30,31] can partly explain the selection of facets but cannot explain the role of Cu additives in the size reduction and shape anisotropy (that is, an aspect ratio not equal to one).

In this work, we conduct a systematic study into the Cu^{2+}-assisted growth of gold nanobars to understand the roles of Cu^{2+} additives in controlling the shape, size, and structure using transmission electron microscopy. We propose a growth mechanism based on the resulting experimental evidence. It is the copper present at the surface of the nanobars that modifies the surface diffusion of gold atoms, resulting in the observed size reduction and shape anisotropy.

Results

Characterization of Cu^{2+}-assisted gold nanobars

The gold nanobars are synthesized using the seed-mediated approach, according to the method reported previously.[22] Gold seeds synthesized as outlined here are well known to be primarily (>80%) single crystals, 1.5–2 nm in size, with cuboctahedral morphology.[21,32] Growth of these seeds in the absence of metal additives (with sufficient gold precursor) leads to the formation of larger (>45 nm edge length) cubes,[18,33] spheres,[34] or, with high CTAB concentrations, penta-twinned nanorods.[35,36] The products grown in the presence of copper ions (as Cu^{2+}, at a

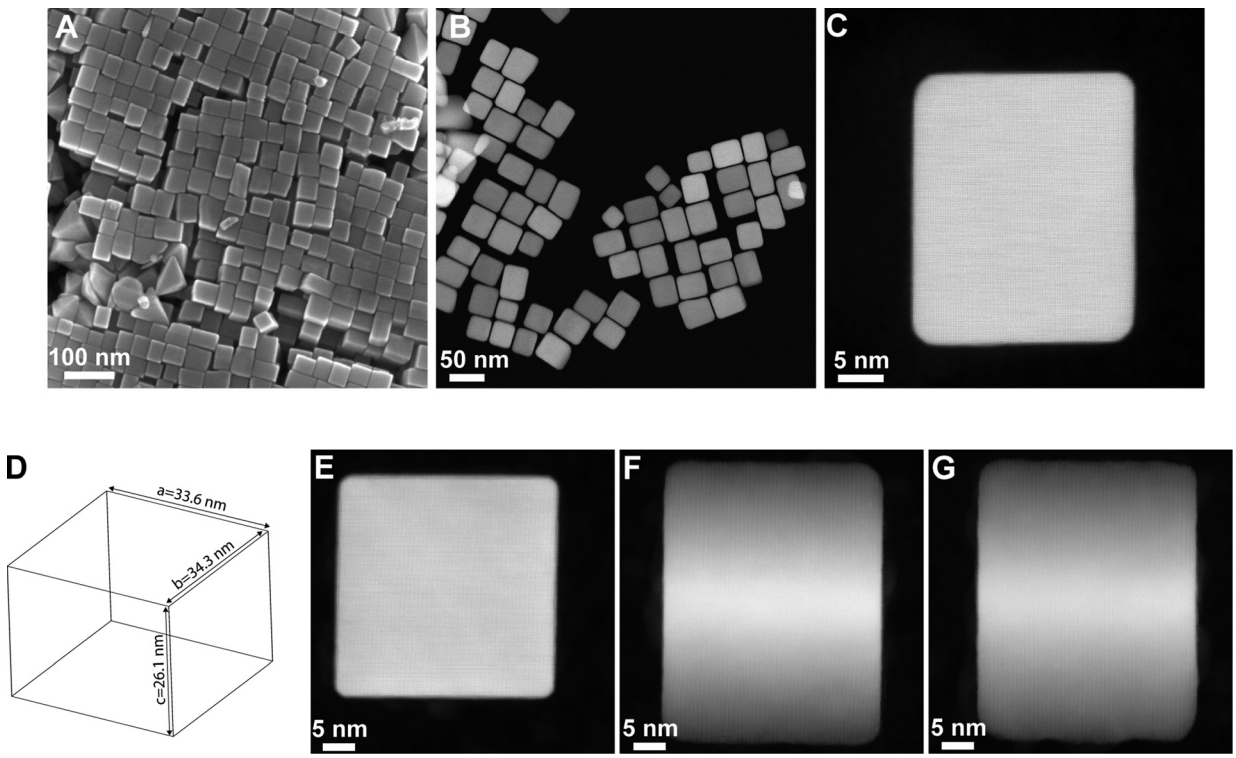

Fig. 1 Characterization of the final products of Cu^{2+}-assisted synthesis of gold nanobars ($[Cu^{2+}]$ = 19.2 μM). (A) An overview SEM image. (B) An overview low magnification HAADF-STEM image. (C) An HAADF-STEM image of a representative nanobar with the electron beam parallel to the ⟨001⟩ direction. (D) reconstructed nanobar model based on the edge length measurements of a representative gold nanobar observed in different zone axes: (E) ⟨001⟩, (F) ⟨011⟩, (G) $\langle 01\bar{1} \rangle$. This nanobar is projected as a square in the ⟨001⟩ direction but the 3rd dimension of the nanobar, calculated from the length of the diagonal line, is significantly smaller than the other two sides, as shown in (D).

concentration of 19.2 μM) are shown in Fig. 1 (and Fig. S1, ESI†) and the absorption spectrum is shown in Fig. 2. The majority of particles are cuboids, with right bipyramids and rod-like byproducts also observed, consistent with previous reports.[22] Cuboid particles account for 88% of the final product (based on the shape statistics of 975 nanoparticles, detailed in Table S2, ESI†). The yield was consistently >80% across multiple identical synthesis. Of those nanoparticles identified as cuboids, a high percentage (quantified later) are found to be nanobars (*i.e.* AR ≠ 1) when viewed in the ⟨001⟩ direction, as apparent from the scanning electron microscopy image (SEM) in Fig. 1(A) and high angle annular dark-field scanning transmission electron microscopy (HAADF-STEM) images in Fig. 1(B) and (C).

The nanobars have an average aspect ratio (AR), length/width, of 1.2 ± 0.2, as measured in projection. The average edge length of nanobars was measured to be 28 ± 3 nm for the shorter dimension (width) and 34 ± 5 nm for the longer dimension (length). These sizes are significantly smaller than that of symmetric cubes grown in the absence of Cu^{2+}.[4,6] The absorption spectrum displays a single, although asymmetric, plasmon resonance at λ_{max} = 527 nm. The asymmetry observed is attributed to the differences in length and width of the cuboids, with the reduction in symmetry causing splitting of the plasmon resonance, along with contributions to the spectrum from the byproduct/s. A small peak is also observed in the near-infrared region as a consequence of the small percentage of nanorod byproducts formed (Fig. S3(A), ESI†).

We notice that in the Cu^{2+}-assisted gold nanobar synthesis, a significant number of nanobars appear to have an AR close to 1, (*i.e.* they appear square in projection). However, a single TEM image is a two-dimensional projection of a three-dimensional shape, so only 2 dimensions of the nanocuboid can be determined from a single image, with the 3rd dimension unknown. The 3rd dimension can be measured by tilting the cuboid to the ⟨011⟩ zone axis, as shown for example for two representative nanocuboids in Fig. 1(D) (and Fig. S2, ESI†). The 2 sides of the nanocuboid in Fig. 1(E) are a = 33.6 nm and b = 34.4 nm, respectively. Tilting this nanocuboid to the ⟨011⟩ zone axis (Fig. 1(F) and (G)), gives a length of 43.1 nm, from which the 3rd dimension is calculated to be 26.1 nm using simple geometry. Hence, this is not a cube but a "square" nanobar ($a \sim b \neq c$, in other words, 2 parallel square faces and 2 pairs of parallel rectangular faces). Another example is given in Fig. S2 (ESI†) where a = 29.3 nm, b = 29.6 nm, c = 33.4 nm. It can be concluded that the nanocuboids synthesized in the presence of Cu^{2+} are nanobars (AR ≠ 1), even for those which appear to be near perfect cubes in projection in TEM and SEM images. To achieve this, there must be different growth rates for at least 1 of the 3 pairs of nominally symmetry-equivalent {100} facets, so that the particle symmetry is lowered.[6,18] Finally, we also observe that the nanobars are near-perfect cuboids, without corner truncations, except for slight curvatures at vertices/corners (Fig. 1(F) and (G), orientated in ⟨011⟩ directions).

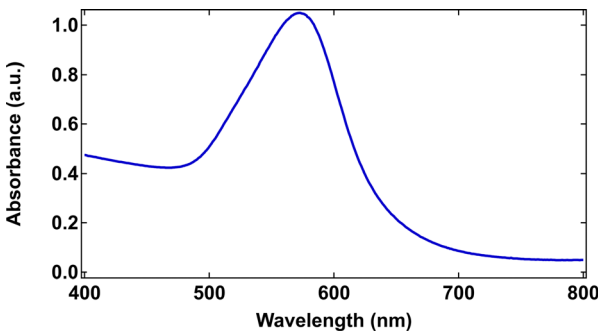

Fig. 2 UV-vis spectrum of "optimized" cube sample, with [Cu^{2+}] = 19.2 μM $CuCl_2$ added, grown for 48 hours.

For [Cu^{2+}] = 19.2 μM, the major synthetic product is the nanobar geometry described above, with right bipyramids (along with a small percentage of triangular particles), rod-like particles and others (mostly spheres) as byproducts.[22] To examine whether the Cu^{2+} concentration affects the shape and/or size, we varied the Cu^{2+} concentration in fine increments from 14 to 25 μM. Absorption spectra of these are shown in Fig. S3(A) and (B) (ESI†). Small shifts in the plasmon resonance around $\lambda_{max} \sim$ 527 nm are observed, with a distinct broadening on the low energy side of the peak for the sample with the highest copper concentration (24.9 μM). Size analysis of 2D-projected TEM/SEM images shows that there is only a very small difference between the average aspect ratios of the nanocuboids synthesized with the different Cu^{2+} concentrations, ranging from 1.1 ± 0.1 to 1.2 ± 0.2 (Fig. S4 and Table S1, ESI†). However, as the 'aspect ratio' is only a measure of 2 of the 3 nanocuboid dimensions, for some proportion of these the longest (or shortest) dimension will not be measured depending on their orientation on the substrate. Therefore, the aspect ratio must be considered in combination with the frequency with which different lengths and widths occur. These statistics show that the nanocuboids synthesized at [Cu^{2+}] = 19.2 μM have a slightly higher proportion of nanocuboids with larger aspect ratio (Fig. S5, ESI†). The distributions in nanocuboid length and width also exhibit similar trends where a higher proportion of nanocuboids have larger lengths/widths (Fig. S6, ESI†) at [Cu^{2+}] = 19.2 μM.

The most notable effect of varying the Cu^{2+} concentration is the change in yield for the different nanoparticle morphologies (Fig. S4 and Table S2, ESI†). Decreasing or increasing Cu^{2+} concentration leads to notable reductions in the yield of nanocuboids. At higher Cu^{2+} concentrations (24.9 μM) the yield of right bipyramids, which incorporate a single twin plane, is increased. The increase in shape polydispersity of this colloid is consistent with the observed broadening of the absorption spectrum (Fig. S3(A), ESI†). Both the right bipyramids and rod-like byproducts have twinned crystal structures, with one and five twin-planes respectively. The optimum Cu^{2+} concentration for maximizing nanocuboid yield is 19.2 μM.

Shape evolution of Cu^{2+}-assisted gold nanobars

The seed particles used for Cu^{2+}-assisted gold nanobars have been previously characterized as single-crystal cuboctahedral seeds.[21,32] Therefore, a symmetry-breaking event must occur in the transition from these isotropic seeds to anisotropic nanobars

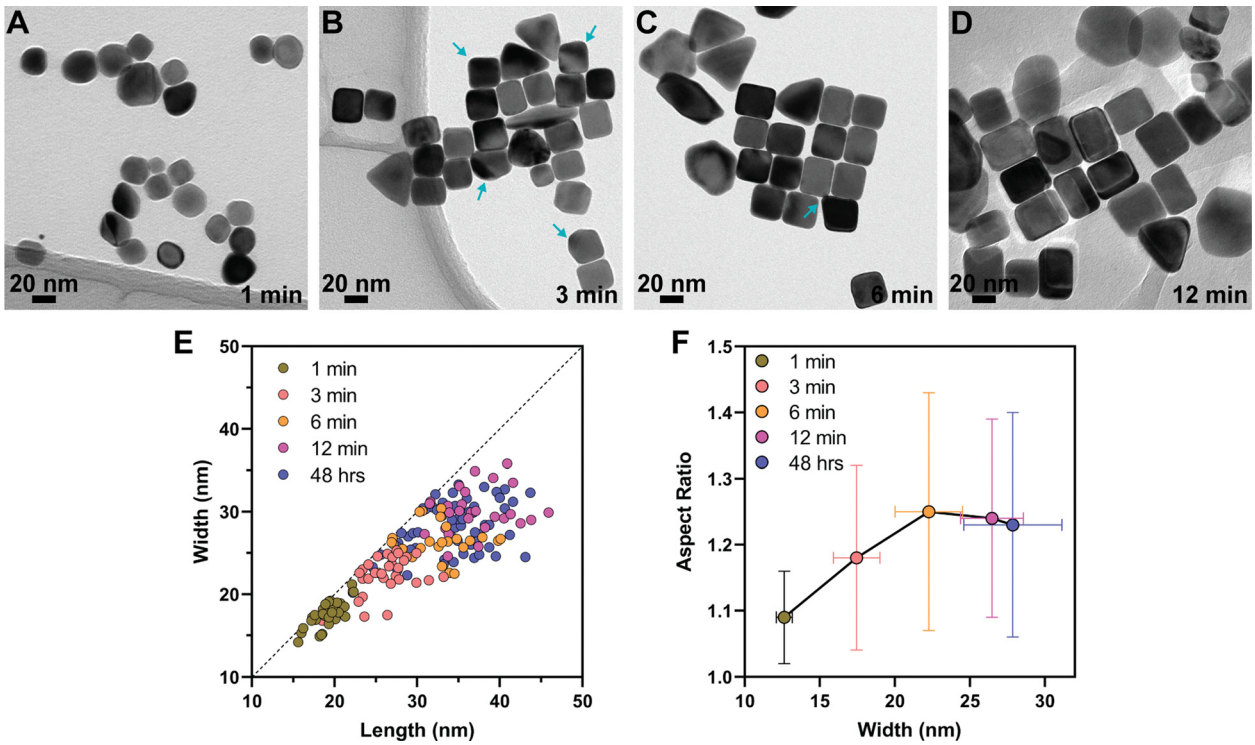

Fig. 3 TEM images of Cu^{2+}-assisted synthesis of gold nanobars with the growth time of seed particles in the growth solution for (A) 1 min, (B) 3 min, (C) 6 min and (D) 12 min. (E) Measurements of the size and aspect ratio of particles orientated in the ⟨001⟩ direction. Each dot represents a nanobar, and the dashed line indicates aspect ratio equals to 1. (F) Summary of the change of aspect ratio as a function of particle size. Blue arrows in (B) and (C) indicate corner bumps. (The bright detached "ghost images" accompanying the thicker particles arise from diffracted beams which produce dark-field images that are focused onto a different plane than that of the undiffracted zero-beam, due to the aberrations in the lower objective pole-piece.)

during the growth. In order to identify at which stage anisotropic growth begins, we studied the nanoparticles at different times. Specifically, following the addition of the seed particles into the growth solution, particles were removed from the growth solution at different growth times and characterized by TEM. A shape evolution pathway of nanobars can thus be established based on the high resolution TEM (HRTEM) images (Fig. 3) along with UV-vis-NIR spectra. At 1 min, the particles are not yet cuboids, and can at best be roughly described as quasi-spherical or quasi-elliptical. Some irregularity is observed giving deviations from perfect spheres or ellipsoids (Fig. 3(A)). At 3 min, the quasi-spherical/ellipsoidal particles have transformed into a bar with clear {100} surface facets (Fig. 3(B)). Irregular surface "bumps" are prevalent at this stage and are predominately localized at vertices/corners as indicated by cyan arrows, with an apparently random distribution across both number of corners and sizes. Individual bar particles at 1 min and 3 min were examined in more detail along the ⟨001⟩ zone axis, further confirming the existence of corner bumps (Fig. S7, ESI†). At 6 min, the nanobars have further increased in size, and the irregular bumps are less frequent, although they are still sometimes observed (Fig. 3(C)). Following further growth, at 12 min, sharp corners and vertices are observed (Fig. 3(D)). No bumps at corners are present, at least in the careful examination of 28 individual nanobars at 12 min (we cannot exclude the possibility that there may be an extremely small percentage of nanobars that possess corner bumps, but we did not observe any). At 12 min, the size and shape of gold nanocubes are close to those of the final products at 48 hours (Fig. S8 and S9, ESI†). We notice a slight change in peak position (blue shift) and peak intensity after 8 min, which is attributed to the minor change in nanocuboid morphology, such as the small size reduction (Fig. 3(F)) or corner sharpness (Fig. S9, ESI†).

Based on the HRTEM images of 114 particles (>24 particles for each time point) precisely oriented to the ⟨001⟩ zone axis, the changes in the size and aspect ratio with growth time are summarized in Fig. 3(E) and (F). Significantly, the average aspect ratio at 1 min is already not quite equal to 1 (1.09). That is, anisotropic growth has already commenced, well before cuboids are formed. The aspect ratio increases gradually from 1.09 to 1.25 in the period 1 min to 6 min and then plateaus, with little change up to 48 hours of growth. Consistent with these changes, the absorption spectrum changes only minimally during the growth, with a small narrowing of the resonance accompanied by an increase in the absorption over this time (Fig. S3(C), ESI†). The results suggest that the Cu^{2+}-assisted anisotropic growth can most likely be attributed to a process of surface deposition and diffusion, instead of a product of coalescence, *e.g.* orientated attachment.[37,38] To investigate this further, we study the role of diffusion rate and the influence of Cu^{2+} additive, as described in the following sections.

As a side note, the nanobars are meta-stable, and reshape to more thermodynamically stable spheres within two weeks. This occurs both in the original growth solution, as well as in solution with lower CTAB concentration ($\sim$1 mM) and minimal Cu^{2+} (*i.e.* following cleanup). The absorption spectrum of the colloid after two weeks, Fig. S3(D) (ESI†), shows a blue-shift of the plasmon resonance to $\lambda_{max} \sim 540$ nm as expected for small, isotropic spheres.

Impact of diffusion rate on Cu^{2+}-assisted gold nanobars

Because surface diffusion is a thermally promoted motion,[39] we modified the growth temperature to determine the role of the surface diffusion rate on the shape anisotropy of Cu^{2+}-assisted gold nanobars. The growths were carried out at 28 °C (standard temperature) and 38 °C respectively.

Fig. 4(A) shows the morphology of nanobars synthesized at 38 °C. They retain the nanobar shape but are slightly larger with a lower average aspect ratio of 1.08 ± 0.07, compared to that of the particles synthesized at 28 °C (1.2 ± 0.2) (Fig. 4(B)). A two-tail *t*-test was conducted against aspect ratio to determine whether there is a statistically significant difference between the two syntheses. Taking 0.05 as the criterion for acceptance, the gold nanobars at different temperatures are undoubtedly different in aspect ratio ($1.08 \times 10^{-12} \ll 0.05$). The slower surface diffusion rate expected at 28 °C would benefit the shape anisotropy of gold nanobars.

Varying the addition time of Cu^{2+} additives

The timing of the addition of the diluted seeds into the growth solution was varied (at 0, 2, 5 min after addition of Cu^{2+} additives, respectively). The statistical shape yield analysis obtained from SEM images shows that the yield of nanobars decreases from 85% to 64%, as the time interval between addition of Cu^{2+} additives and seeds increase (Table S3 and Fig. S10, ESI†). This corresponds to an increased percentage of by-products, which are primarily RBPs but also includes a small amount of rod-like particles and spheres. This suggests it is favorable for Cu^{2+} additives to remain "available" within the solution, not associated with slowly diffusing CTAB micelles.

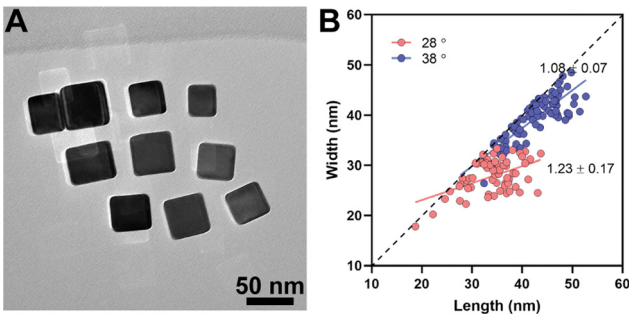

Fig. 4 (A) overview TEM image of Cu^{2+}-assisted gold nanobars synthesized at 38 °C. (B) size analysis of Cu^{2+}-assisted gold nanobars synthesized at 28 °C (64 nanobars) and 38 °C (89 nanobars), respectively. Statistics from 2D projections of the particles.

Absence of Cu^{2+} additives

To further investigate whether Cu^{2+} ions are critical for the symmetry breaking of gold nanocube, the synthesis was carried out without Cu^{2+} additives. The two syntheses are compared in Fig. 5. The presence of Cu^{2+} leads to a dark violet dispersion after 48 hours of growth, while in the absence of Cu^{2+}, the dispersion is magenta, reflecting the differences in particle shape and size between the two syntheses (Fig. 5(A)). The latter also leads to the nanoparticle morphologies of cuboids, RBPs and rods,[40] however the yield of nanocuboids based on the analysis of 260 particles is 48%, lower than with Cu^{2+} (Fig. 5(B) and Fig. S12, ESI†). More interestingly, Fig. 5(C) shows that the edge length of the nanocuboids in the absence of Cu^{2+} is around 50 nm, almost twice that of Cu^{2+}-assisted gold nanobars, and furthermore, the nanocuboids incorporate lamellar twin planes.[40]

The cuboid edge length was measured for the two syntheses and plotted in Fig. 5(C). With the assistance of Cu^{2+}, the dots deviate from the dashed line (AR = 1) clearly indicate the shape anisotropy of the cuboids. Those with AR close to 1 in Fig. 1(D)–(G) have been proven to be square bars. If we assume for a moment that all the nanocuboids synthesized with Cu^{2+} are in fact square nanobars, then we might expect $\sim$1/3 to image as a square in the ⟨001⟩ projection with an AR = 1 (*i.e.* 1/3 of the square nanobar facets are square, hence $\sim$1/3 of nanobars might lie on their square face, possibly fewer if the length is significantly greater than the width making the nanobar less stable if it is supported on its smaller side). In practice, $\sim$28% of the 64 nanocuboids measured in Fig. 5(C) have an AR $\sim$1 to 1.1. It is therefore estimated that almost all the nanocuboids synthesized in the presence of copper are nanobars, with $a \sim b \neq c$ even for those which appear to be cubes in projection in TEM and SEM images.

In contrast, all the nanocuboids synthesized in the absence of Cu^{2+} were measured to have AR = 1 (with variations between 1 and 1.05), that is, they are nanocubes, not bars. No nanobars were observed, even after tilting the specimen as described above.

In conclusion, this comparison strongly suggests that Cu^{2+} additives are critical both for the size reduction and symmetry breaking required to deliver small gold nanobars, relative to the Cu^{2+}-free synthesis of large gold nanocubes (Fig. 5).

Discussion

The role of Cu^{2+} ions in anisotropic growth

From the results presented in Fig. 3, three critical conclusions can be made regarding the anisotropic growth of Cu^{2+}-assisted gold nanobars. Firstly, anisotropic growth of gold nanobars occurs in the first 6 minutes of growth. Secondly, the particle shape evolves from a quasi-spherical morphology to a bar, accompanied by the appearance and disappearance of surface bumps at vertices/corners within this period. Thirdly, after 6 minutes, with the disappearance of surface bumps and the completion of the shape transition, nanobars only grow in size but not in aspect ratio. These growth steps are described schematically in Fig. 6(B) and below:

(1) Once seed particles with an initial cuboctahedral shape and alternating {111} and {001} facets are added into the

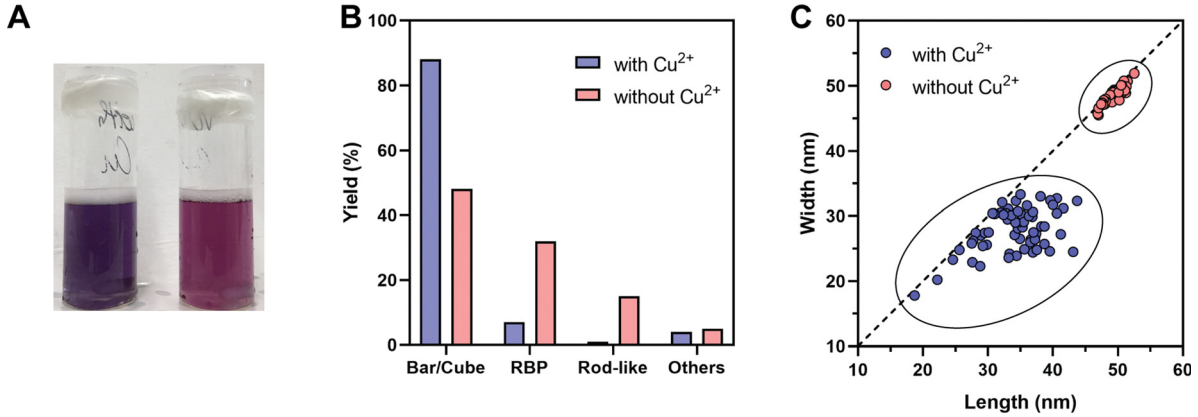

Fig. 5 (A) Final solutions synthesized with Cu^{2+} additives (left) and without Cu^{2+} additives (right). (B) Statistics of shape yields. (C) Statistics of edge lengths of nanobars/nanocubes based on the analysis of 64/51 gold nanobars/nanocubes, respectively, precisely orientated to the ⟨001⟩ zone axis. Final products/solutions refer to the seed particles grown in the growth solution for 48 hours. The dashed line in (C) indicates where the aspect ratio equals to 1.

growth solution, gold atoms quickly deposit on the surface of the seed particles. This deposition happens faster on the {111} facets due to the passivation of {001} facets by surfactants (CTAB in our case),[18] leading to the shape transition from cuboctahedra to quasi-spheres/quasi-ellipsoids.

(2) Further rapid selective deposition on corners results in the formation of surface bumps. A crucial parameter in this step is the relatively slow surface diffusion of gold atoms. As a result, the gold atoms or a cluster of gold atoms deposited on the {111} facets can only diffuse slowly to the lower energy {001} facets, leading to a 'build up' of gold atoms and facilitating the formation of "corner" bumps. In other words, relative to the deposition rate of gold atoms, a fast surface diffusion of depositing atoms results in round corners (Fig. 6(B), top row), with the deposited atoms having sufficient time to diffuse to adjacent facets, preventing corner atom "buildup". The diffusion of gold atoms from corners to adjacent {100} facets is therefore equivalent for these adjacent {100} facets, ensuring the growth rates of cuboids in all the ⟨100⟩ directions is equivalent. However, a slower surface diffusion results in corner atom "buildup" and the formation of asymmetric corner shapes (*i.e.* corner bumps). The slower surface diffusion from the corner bumps results in the atoms diffusing to the closer of the {100} facets, making the growth rate of the cuboid in that specific <100> direction faster than other symmetry-equivalent ⟨100⟩ directions (Fig. 6(B), bottom row). The formation of the corner bumps appears to occur randomly on one corner or some corners, as shown in Fig. 6(A) and Fig. S7 (ESI†). Their random distribution and size is attributed to the rapid growth rate of the nanoparticles.

It is the asymmetry in the number of atoms deposited on the different corners which drives the differential growth of the facets and therefore the symmetry breaking.

(3) With the depletion of gold atoms in the solution, the growth slows down, and the atoms at the bump sites diffuse gradually to the nearest {001} facets. The asymmetric distribution of surface bumps at different corners leads to non-equivalent growth rates in different ⟨001⟩ directions.

(4) Given that the deposition of gold atoms on corners becomes much slower than the rate of diffusion, surface bumps disappear entirely, and meanwhile, no anisotropic growth is involved in the subsequent growth. After a full growth, anisotropic gold nanobars are produced by sharpening corners due to the energy-efficient preservation of {001} facets.[41]

The requirement of slow surface diffusion in the anisotropic growth is supported by the higher growth temperature in Fig. 4. When the rate of surface diffusion is increased by increasing growth temperature, the formation of surface bumps is largely retarded due to the more immediate diffusion of deposited gold atoms from the corner {111} facets to the neighbouring facets. Gold nanobars with an average AR larger than 1 are observed in the final products, but they possess a lower degree of asymmetry, with average AR = 1.1, compared to the products formed for growth at lower temperatures where surface diffusion will be slower.

This anisotropic growth pathway (Fig. 6(B), lower) occurs only in the presence of Cu^{2+} additives, and a plausible atomic-level mechanism to account for the role of Cu^{2+} additives is illustrated in Fig. 6(C). Underpotential deposition (UPD) of Cu has been reported to occur on Au (111) and Au (100) facets,[27,30] similar to that proposed for Ag^{+} additives.[25] Once deposited on the Au surface, the existence of Cu layer(s) and excess gold ions in solution create the conditions required for galvanic replacement. The self-sustaining cycle involves three steps: (1) UPD of Cu (from Cu^{2+} in solution) on the Au {111} facets; (2) galvanic replacement of Cu by Au^{+} ions; (3) Cu^{2+} ions are reduced back onto the Au {111} facets. The result of this process is a Cu metal layer(s) on the surface of the Au nanobars. The presence of Cu^{0} on the surface of Au nanoparticles due to Cu^{2+} UPD has been shown previously using X-ray photoelectron spectrometer (XPS).[30,31]

In Fig. 6(D)–(G), energy dispersive X-ray (EDX) analyses confirm the existence of copper on the surface of the Cu^{2+}-assisted gold nanobars. For growth of nanoparticles in the presence of copper, Cu UPD layers can form on the surface of gold nanobars, with the result that gold atoms deposited must diffuse across a copper surface instead of a gold surface (in the

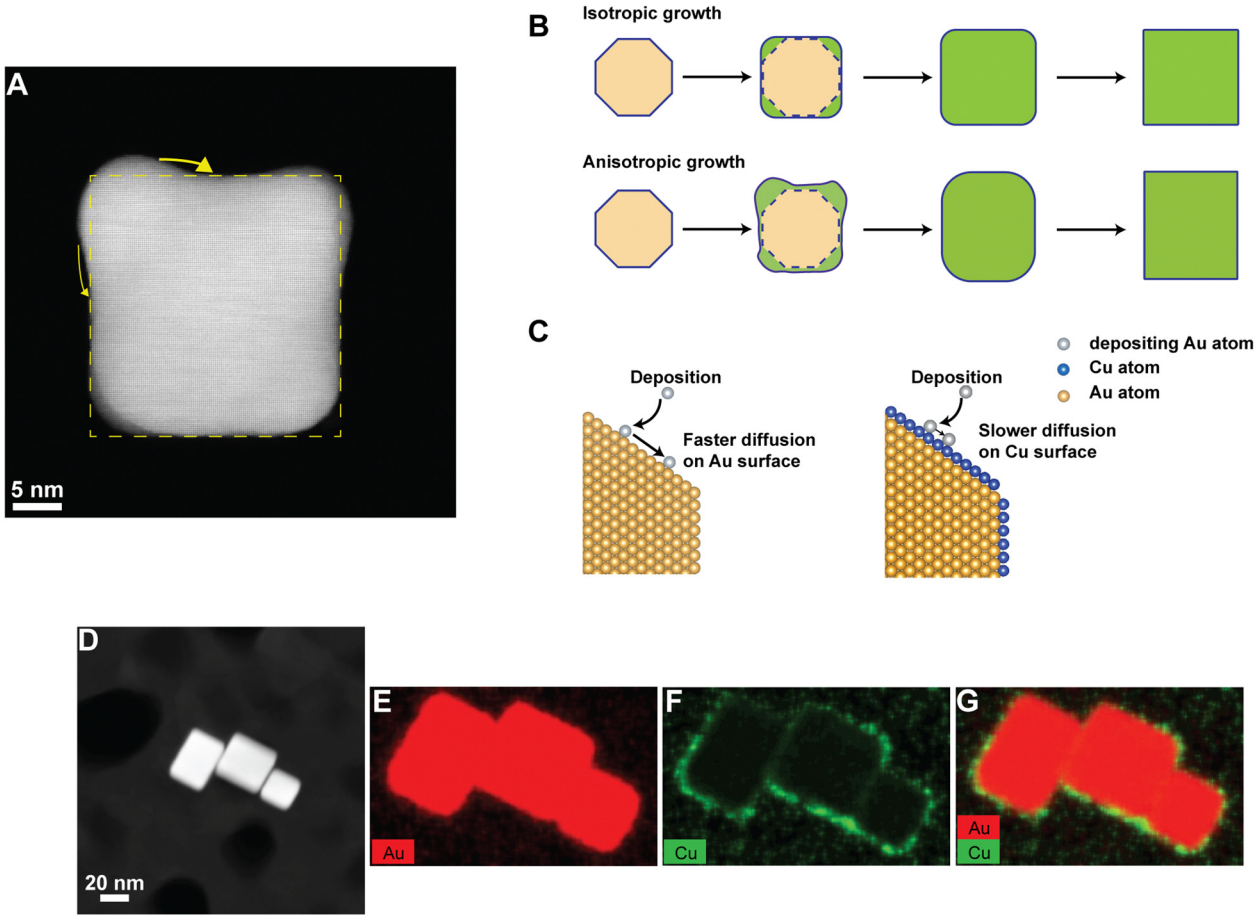

Fig. 6 (A) A representative Cu^{2+}-assisted gold nanobar sampled at 3 min growth time. (B) Schematic illustration of the sequence leading to isotropic of gold nanocubes (top row) and anisotropic growth in Cu^{2+}-assisted gold nanobars (bottom row). (C) Schematic illustration of the slower surface diffusion of depositing Au atoms when the nanoparticle surface is covered by Cu layer(s). (D)–(G) Energy dispersive X-ray (EDX) STEM mapping of Cu^{2+}-assisted gold nanocubes. (D) HAADF image, (E) Au map, (F) Cu map and (G) Au and Cu map.

absence of Cu^{2+}).[41,42] The diffusion of gold atoms on the copper surface is likely to be slower than on a gold surface. Although the solute diffusion rate of gold atoms on a gold surface and copper surface has not been reported, the relative diffusion rate is likely to be related to the binding energies: E_{Au-Au} (221.3 kJ mol^{-1}) < E_{Au-Cu} (232 kJ mol^{-1}),[43] or the adatom-vacancy formation energies on the {111} surfaces: E_{Au} (1.009 eV) < E_{cu} (1.329 eV).[44] In the presence of copper ions, the slower surface diffusion rate contributes to the formation of surface bumps and ultimately, the shape anisotropy of the final products.

The role of Cu^{2+} ions in size reduction

It has been proposed that the transition size from a cuboctahedron to a nanocube is determined by the surface diffusion distance which is proportional to the surface diffusion rate ($\Delta x = 2D_s t^{0.5}$, where D_s denotes the surface diffusion rate and t denotes the time).[6] The Au atoms deposited on {111} facets can self-diffuse to {100} facets, retaining the cuboctahedral shape. Once the particle size becomes larger than the surface diffusion distance, this diffusion process becomes more difficult, and the accumulation of atoms on {111} facets lead to the transition to a cubic shape (we call the size of the particle at which this occurs the "transition size"). A long surface diffusion distance at a faster surface diffusion rate thus results in a larger transition size and a larger final product. In our results, the transition from a cuboctahedron to a cuboid, in the absence of Cu^{2+} additives, occurs at a particle size of 23–25 nm (Fig. S11(A)–(C), ESI†), and the ultimate size of the gold nanocubes is ~48 nm (Fig. S12, ESI†), consistent with the size reported in the literature.[6,40] In stark contrast, the Cu^{2+}-assisted gold nanobars have a transition size of 17–19 nm (Fig. 3, and Fig. S11(D), (E), ESI†) and a final size of 28–34 nm. The reduction in both final size and transition size can be explained if the surface diffusion rate is slower in the presence of Cu^{2+} additives. This is further supported by the observation that a higher growth temperature leads to the faster surface diffusion and thus longer surface diffusion distance, resulting in gold nanobars with a larger size than the gold nanobars grown at a lower growth temperature (Fig. 4).

Conclusions

In summary, we show that Cu^{2+} additives intervene fundamentally in the growth process to produce smaller gold nanobars, rather than larger gold nanocubes, that is, breaking symmetry

and reducing sizes. Cu UPD layers formed on the surface of gold nanocubes slows the surface diffusion of Au adatoms from 'corner' {111} facets to side {001} facets, facilitating the growth of randomly distributed and differently sized surface bumps at corners. These subsequently diffuse to adjacent facets, resulting in anisotropic growth as a consequence of the random nature of the deposits. This also explains the size reduction in the presence of Cu^{2+} additives. Our observations provide insights into the role of metallic additives in the synthesis of metal nanoparticles and the correlations between metallic additives and anisotropic growth.

Conflicts of interest

The authors declare no competing financial interest.

Acknowledgements

This work was supported by the Australian Research Council (ARC) Discovery Project number DP160104679 and the ARC Centre of Excellence in Exciton Science, CE170100026. We thank the Monash Centre for Electron Microscopy (MCEM) for access to the transmission electron microscopes funded by ARC grants LE0454166 and LE110100223 and MCEM staff for their expert assistance. W. L. thanks the support of the Australian Government Research Training Program (RTP) scholarship. W. T. thanks the Australian Department of Education and Monash University for the IPRS and APA scholarships. The authors thank Sian Franklin and Miri Shiradski for their roles in gold nanobar syntheses.

Notes and references

1 H. Häkkinen, M. Moseler, O. Kostko, N. Morgner, M. A. Hoffmann and B. V. Issendorff, Symmetry and Electronic Structure of Noble-Metal Nanoparticles and the Role of Relativity, *Phys. Rev. Lett.*, 2004, **93**(9), 1–4.

2 Y. Sun and Y. Xia, Shape-Controlled Synthesis of Gold and Silver Nanoparticles, *Science*, 2002, **298**(5601), 2176–2179.

3 W. Niu, S. Zheng, D. Wang, X. Liu, H. Li, S. Han, J. Chen, Z. Tang and G. Xu, Selective Synthesis of Single-Crystalline Rhombic Dodecahedral, Octahedral, and Cubic Gold Nanocrystals, *J. Am. Chem. Soc.*, 2009, **131**(2), 697–703.

4 D. Seo, C. P. Ji and H. Song, Polyhedral Gold Nanocrystals with Oh Symmetry: From Octahedra to Cubes, *J. Am. Chem. Soc.*, 2006, **128**(46), 14863–14870.

5 A. Umar, J. Lee, J. Dey and S. M. Choi, Seedless Synthesis of Monodisperse Cuboctahedral Gold Nanoparticles with Tunable Sizes, *Chem. Mater.*, 2016, **28**(14), 4962–4970.

6 E. Dovgolevsky and H. Haick, Direct Observation of the Transition Point between Quasi-Spherical and Cubic Nanoparticles in a Two-Step Seed-Mediated Growth Method, *Small*, 2008, **4**(11), 2059–2066.

7 L. Zhang, Y. Zhang, J. Ahn, X. Wang and D. Qin, Defect-Assisted Deposition of Au on Ag for the Fabrication of Core-Shell Nanocubes with Outstanding Chemical and Thermal Stability, *Chem. Mater.*, 2019, **31**(3), 1057–1065.

8 C. F. Hsia, M. Madasu and M. H. Huang, Aqueous Phase Synthesis of Au–Cu Core–Shell Nanocubes and Octahedra with Tunable Sizes and Noncentrally Located Cores, *Chem. Mater.*, 2016, **28**(9), 3073–3079.

9 J. Zhu, F. Zhang, B. B. Chen, J. J. Li and J. W. Zhao, Tuning the Shell Thickness-Dependent Plasmonic Absorption of Ag Coated Au Nanocubes: The Effect of Synthesis Temperature, *Mater. Sci. Eng., B*, 2015, **199**, 113–120.

10 K. D. Gilroy, H. C. Peng, X. Yang, A. Ruditskiy and Y. Xia, Symmetry Breaking during Nanocrystal Growth, *Chem. Commun.*, 2017, **53**(33), 4530–4541.

11 Z. Guan, S. Li, P. B. S. Cheng, N. Zhou, N. Gao and Q. H. Xu, Band-Selective Coupling-Induced Enhancement of Two-Photon Photoluminescence in Gold Nanocubes and Its Application as Turn-on Fluorescent Probes for Cysteine and Glutathione, *ACS Appl. Mater. Interfaces*, 2012, **4**(10), 5711–5716.

12 X. Wu, T. Ming, X. Wang, P. Wang, J. Wang and J. Chen, High-Photoluminescence-Yield Gold Nanocubes: For Cell Imaging and Photothermal Therapy, *ACS Nano*, 2010, **4**(1), 113–120.

13 Y. Xia, W. Li, C. M. Cobley, J. Chen, X. Xia, Q. Zhang, M. Yang, E. C. Cho and P. K. Brown, Gold Nanocages: From Synthesis to Theranostic Applications, *Acc. Chem. Res.*, 2011, **44**(10), 914–924.

14 J. E. Park, S. Kim, J. Son, Y. Lee and J. M. Nam, Highly Controlled Synthesis and Super-Radiant Photoluminescence of Plasmonic Cube-in-Cube Nanoparticles, *Nano Lett.*, 2016, **16**(12), 7962–7967.

15 D. Lee and S. Yoon, Gold Nanocube-Nanosphere Dimers: Preparation, Plasmon Coupling, and Surface-Enhanced Raman Scattering, *J. Phys. Chem. C*, 2015, **119**(14), 7873–7882.

16 P. Matteini, M. De Angelis, L. Ulivi, S. Centi and R. Pini, Concave Gold Nanocube Assemblies as Nanotraps for Surface-Enhanced Raman Scattering-Based Detection of Proteins, *Nanoscale*, 2015, **7**(8), 3474–3480.

17 J. E. Park, Y. Lee and J. M. Nam, Precisely Shaped, Uniformly Formed Gold Nanocubes with Ultrahigh Reproducibility in Single-Particle Scattering and Surface-Enhanced Raman Scattering, *Nano Lett.*, 2018, **18**(10), 6475–6482.

18 T. K. Sau and C. J. Murphy, Room Temperature, High-Yield Synthesis of Multiple Shapes of Gold Nanoparticles in Aqueous Solution, *J. Am. Chem. Soc.*, 2004, **126**(28), 8648–8649.

19 C.-J. Huang, P.-H. Chiu, Y.-H. Wang, W. R. Chen and T. H. Meen, Synthesis of the Gold Nanocubes by Electrochemical Technique, *J. Electrochem. Soc.*, 2006, **153**(8), D129.

20 C. J. Johnson, E. Dujardin, S. A. Davis, C. J. Murphy and S. Mann, Growth and Form of Gold Nanorods Prepared by Seed-Mediated, Surfactant-Directed Synthesis, *J. Mater. Chem.*, 2002, **12**(6), 1765–1770.

21 M. Liu and P. Guyot-Sionnest, Mechanism of Silver(I)-Assisted Growth of Gold Nanorods and Bipyramids, *J. Phys. Chem. B*, 2005, **109**(47), 22192–22200.

22 J. Sun, M. Guan, T. Shang, C. Gao, Z. Xu and J. Zhu, Selective Synthesis of Gold Cuboid and Decahedral Nanoparticles Regulated and Controlled by Cu^{2+} Ions, *Cryst. Growth Des.*, 2008, **8**(3), 906–910.
23 B. Nikoobakht and M. A. El-Sayed, Preparation and Growth Mechanism of Gold Nanorods (NRs) Using Seed-Mediated Growth Method, *Chem. Mater.*, 2003, **15**(10), 1957–1962.
24 M. L. Personick, M. R. Langille, J. Zhang and C. A. Mirkin, Shape Control of Gold Nanoparticles by Silver Underpotential Deposition, *Nano Lett.*, 2011, **11**(8), 3394–3398.
25 M. J. Walsh, W. Tong, H. Katz-Boon, P. Mulvaney, J. Etheridge and A. M. Funston, A Mechanism for Symmetry Breaking and Shape Control in Single-Crystal Gold Nanorods, *Acc. Chem. Res.*, 2017, **50**(12), 2925–2935.
26 G. González-Rubio, L. Scarabelli, A. Guerrero-Martínez and L. M. Liz-Marzán, Surfactant-Assisted Symmetry Breaking in Colloidal Gold Nanocrystal Growth, *ChemNanoMat*, 2020, **6**, 698–707.
27 H. A. Keul, M. Möller and M. R. Bockstaller, Selective Exposition of High and Low Density Crystal Facets of Gold Nanocrystals Using the Seeded-Growth Technique, *CrystEngComm*, 2011, **13**(3), 850–856.
28 W. Liu, H. Zhang, T. Wen, J. Yan, S. Hou, X. Shi, Z. Hu, Y. Ji and X. Wu, Activation of Oxygen-Mediating Pathway Using Copper Ions: Fine-Tuning of Growth Kinetics in Gold Nanorod Overgrowth, *Langmuir*, 2014, **30**(41), 12376–12383.
29 T. Wen, H. Zhang, X. Tang, W. Chu, W. Liu, Y. Ji, Z. Hu, S. Hou, X. Hu and X. Wu, Copper Ion Assisted Reshaping and Etching of Gold Nanorods: Mechanism Studies and Applications, *J. Phys. Chem. C*, 2013, **117**(48), 25769–25777.
30 L. Zhang, Q. Chen, Z. Jiang, Z. Xie and L. Zheng, Cu^{2+} Underpotential-Deposition Assisted Synthesis of Au and Au–Pd Alloy Nanocrystals with Systematic Shape Evolution, *CrystEngComm*, 2015, **17**(29), 5556–5561.
31 L. Zhang, J. Zhang, Q. Kuang, S. Xie, Z. Jiang, Z. Xie and L. Zheng, Cu^{2+}-Assisted Synthesis of Hexoctahedral Au–Pd Alloy Nanocrystals with High-Index Facets, *J. Am. Chem. Soc.*, 2011, **133**(43), 17114–17117.
32 M. J. Walsh, S. J. Barrow, W. Tong, A. M. Funston and J. Etheridge, Symmetry Breaking and Silver in Gold Nanorod Growth, *ACS Nano*, 2015, **9**(1), 715–724.
33 T. Tan, S. Zhang, J. Wang, Y. Zheng, H. Lai, J. Liu, F. Qin and C. Wang, Resolving the Stacking Fault Structure of Silver Nanoplates, *Nanoscale*, 2021, **13**(1), 195–205.
34 J. Rodríguez-Fernández, J. Pérez-Juste, F. J. García De Abajo and L. M. Liz-Marzán, Seeded Growth of Submicron Au Colloids with Quadrupole Plasmon Resonance Modes, *Langmuir*, 2006, **22**(16), 7007–7010.
35 J. Pérez-Juste, I. Pastoriza-Santos, L. M. Liz-Marzán and P. Mulvaney, Gold Nanorods: Synthesis, Characterization and Applications, *Coord. Chem. Rev.*, 2005, **249**(17–18 SPEC. ISS.), 1870–1901.
36 M. Grzelczak, J. Pérez-Juste, P. Mulvaney and L. M. Liz-Marzán, Shape Control in Gold Nanoparticle Synthesis, *Chem. Soc. Rev.*, 2008, **37**(9), 1783–1791.
37 L. M. Bronstein, X. Huang, J. Retrum, A. Schmucker, M. Pink, B. D. Stein, B. Dragnea, R. V. December, V. Re, M. Recei, V. April, F. Wang, V. N. Richards, S. P. Shields, W. E. Buhro, Y. Jin, Q. Yi, Y. Ren, X. Wang, Z. Ye, J. Chang, E. R. Waclawik, X. Zhong, Y. Feng, Y. Zhang, I. Lieberwirth, W. Knoll, D. Ito, S. Yokoyama, T. Zaikova, K. Masuko, J. E. Hutchison, D. Li, M. H. M. H. Nielsen, J. R. I. J. R. I. Lee, C. Frandsen, J. F. Banfield and J. J. De Yoreo, Direction-Specific Interactions Control Crystal Growth by Oriented Attachment, *Science*, 2012, **336**(1), 1014–1018.
38 J. M. Yuk, M. Jeong, S. Y. Kim, H. K. Seo, J. Kim and J. Y. Lee, In Situ Atomic Imaging of Coalescence of Au Nanoparticles on Graphene: Rotation and Grain Boundary Migration, *Chem. Commun.*, 2013, **49**(98), 11479–11481.
39 A. Pedrazo-Tardajos, E. Arslan Irmak, V. Kumar, A. Sánchez-Iglesias, Q. Chen, M. Wirix, B. Freitag, W. Albrecht, S. Van Aert, L. M. Liz-Marzán and S. Bals, Thermal Activation of Gold Atom Diffusion in Au@Pt Nanorods, *ACS Nano*, 2022, **16**(6), 9608–9619.
40 W. Li, W. Tong, A. Yadav, E. Bladt, S. Bals, A. M. Funston and J. Etheridge, Shape Control beyond the Seeds in Gold Nanoparticles, *Chem. Mater.*, 2021, **33**(23), 9152–9164.
41 H. C. Peng, J. Park, L. Zhang and Y. Xia, Toward a Quantitative Understanding of Symmetry Reduction Involved in the Seed-Mediated Growth of Pd Nanocrystals, *J. Am. Chem. Soc.*, 2015, **137**(20), 6643–6652.
42 X. Xia, S. Xie, M. Liu, H. C. Peng, N. Lu, J. Wang, M. J. Kim and Y. Xia, On the Role of Surface Diffusion in Determining the Shape or Morphology of Noble-Metal Nanocrystals, *Proc. Natl. Acad. Sci. U. S. A.*, 2013, **110**(17), 6669–6673.
43 J. A. Dean and N. A. Lange, *Lange's Handbook of Chemistry*, McGraw-Hill, 1992, vol. 4, pp.41–53.
44 P. Stoltze, Simulation of Surface Defects, *J. Phys.: Condens. Matter*, 1994, **6**(45), 9495–9517.

